ELSEVIER

Biophysical Chemistry 123 (2006) 49–57

Biophysical Chemistry

http://www.elsevier.com/locate/biophyschem

Molecular motion of spin labeled side chains in the C-terminal domain of RGL2 protein: A SDSL-EPR and MD study

Sara Pistolesi [a,1], Elisa Ferro [b,1], Annalisa Santucci [b], Riccardo Basosi [a], Lorenza Trabalzini [b], Rebecca Pogni [a,*]

[a] *Department of Chemistry, University of Siena, Via A. Moro, 53100 Siena, Italy*
[b] *Department of Molecular Biology, University of Siena, Via Fiorentina-53100 Siena, Italy*

Received 2 February 2006; received in revised form 31 March 2006; accepted 31 March 2006
Available online 18 April 2006

Abstract

Five singly spin labeled side chains at surface sites in the C-terminal domain of RGL2 protein have been analyzed to investigate the general relationship between nitroxide side chain mobility and protein structure. At these sites, the structural perturbation produced by replacement of a native residue with a nitroxide side chain appears to be very slight at the level of the backbone fold. The primary determinants of the nitroxide side chain mobility are backbone dynamics and tertiary interactions. On the exposed surfaces of α-helices, the side chain mobility is not restricted by tertiary interactions but appears to be determined by backbone dynamics, while in loop sites, the side chain mobility is even higher. For a better understanding of the changes in the EPR spectral line shape, molecular dynamics simulations were performed and found in agreement with EPR spectral data.

Keywords: EPR; Site-directed spin labeling; RGL2 protein; Molecular dynamics

1. Introduction

Knowledge of the structure and dynamics of proteins provides a powerful means to understand key aspects of their function. Site-directed spin labeling (SDSL) has emerged as an effective approach to obtain topographical and dynamical information about both water-soluble and membrane proteins [1–7]. Spin labeling is typically accomplished by cysteine-substitution mutagenesis followed by reaction with a sulfhydryl-specific nitroxide reagent. The one most commonly employed is a methanthiosulfonate derivative that generates the disulfide-linked nitroxide side chain, named R1 (Scheme 1), although other side chains have been employed for specific purposes [8].

The EPR spectrum of a spin labeled side chain in a protein encodes information about dynamical modes of the nitroxide. Such information is important because the nitroxide motion reflects a variety of structural and dynamical features of the protein itself, such as backbone dynamics, bond rotational isomerization within the side chain, modulated by tertiary interactions with its environment and Brownian diffusion. Analysis of the EPR spectrum provides a direct experimental measure for side chain solvent accessibility, determined from the collision frequency of the nitroxide with paramagnetic probes in solution [3], polarity of the local environment deduced from features of the spectrum at low temperature [9], and side chain mobility estimated by the inverse central linewidth and by the spectral second moment [5,10]. While nitroxide side chain accessibility and mobility provide local structural information, global information can be obtained from the introduction of a second paramagnetic center and subsequent determination of interspin distance through detection of magnetic spin–spin interaction [11–17]. The combination of local and global information from SDSL-EPR can provide adequate constraints to model the structure of a protein at the level of the backbone

Abbreviations: RGL2, *R*al*G*DS *l*ike protein-*2*; SDSL, site-directed spin labeling; EPR, electron paramagnetic resonance; MD, molecular dynamics; RBD, Ras binding domain.

* Corresponding author. Tel.: +39 577 234258; fax: +39 577 234239.
E-mail address: pogni@unisi.it (R. Pogni).

[1] The first two authors contributed equally to the work.

0301-4622/$ - see front matter © 2006 Elsevier B.V. All rights reserved.
doi:10.1016/j.bpc.2006.03.021

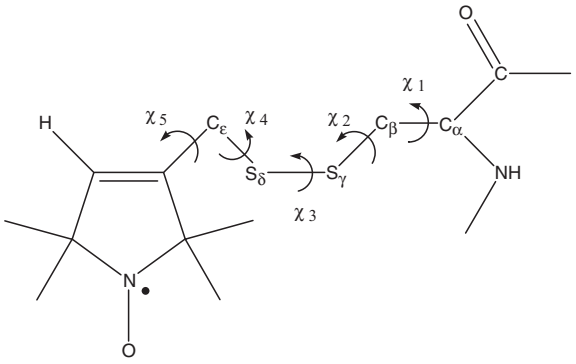

Scheme 1. Structure of the R1 side chain, indicating the dihedral angles χ_1–χ_5.

fold. The SDSL-EPR method has been fruitfully used to determine the structure in bacteriorhodopsin [3,18–20], rhodopsin [21–26], colicin E1 [27], T4 lysozyme [10,11] and the *Streptomyces lividans* K^+ channel [6,28], to cite only some examples.

RGL2 (*R*al*G*DS *l*ike protein-*2*) is a member of the RalGDS family which was isolated as a potential effector for Ras and Ras analogue Rap1b [29,30]. Like the other members of the family, RGL2 contains a carboxyl-terminal domain which binds the GTP ligated form of Ras proteins and an amino-terminal CDC25 homology domain, which has the structural features of a guanine nucleotide exchange factor. On the basis of this two-domain structure, it has been suggested that the members of the RalGDS family are able to couple transduction pathways regulated by Ras or Ras-related proteins with pathways regulated by other small G-proteins. The C-terminal RGL2 fragment which regulates the interaction with Ras proteins contains a region encoding 90 amino acids (RGL2-90) that presents a very high homology with the Ras binding domains (RBDs) of RalGDS family members. On the basis of this evidence, one can suppose that RGL2-90 is the domain of RGL2 directly involved in the interaction with Ras. Therefore, information about structural and dynamical features of RGL2-90 will allow characterization of the Ras binding features of RGL2. In this study, the internal motion of the side chain and the relation between side chain mobility and protein topography of RGL2-90 has been investigated in a manner that reveals the general relationship between structure and EPR line shape. The Electron Paramagnetic Resonance (EPR) analysis has been combined with Molecular Dynamics (MD) simulations. In fact, when attached to a specific protein residue, probe restriction should be well modelled by molecular dynamics simulations. The extent of the narrowing of the nitroxide EPR spectrum is optimally sensitive to the amplitude of nanosecond rotational motions [31–33].

2. Experimental procedures

2.1. Materials

The vector pGEX-4T-3, BL21 *E. coli* strain, glutathione-sepharose 4B resin and isopropyl β-D-thiogalactoside (IPTG) were from Amersham Pharmacia Biotech Ltd. (UK). Protease inhibitors were from Sigma Chemicals and Calbiochem (San Diego, CA, USA). The spin label $C_{10}H_{18}NO_3S_2$ (1-oxyl-2,2,5,5-tetra-methyl-pyrrolidine-3-methyl)methanethiosulfonate was from A.A. Reanal (Budapest). Hi-Trap Desalting columns were from Amersham Pharmacia Biotech. Sucrose was from Sigma Chemicals.

2.2. Plasmid construction

The RGL2-90(647–736) coding sequence was amplified by PCR using primers that created a *Bam*HI site at the 5′ and an *Eco*RI site at the 3′ end, and then ligated into *Bam*HI/*Eco*RI digested pGEX-4T-3 vector.

Cys-less RGL2-90 was created by PCR by substituting the unique native cysteine (C649) with serine. Single cysteine mutants of RGL2-90 lacking native cysteine were produced starting from Cys-Less RGL2-90 by site-directed mutagenesis performed by a two-step PCR amplification using the appropriate mutagenesis primers and then ligated into pGEX-4T-3. All constructs were verified by sequencing.

2.3. Protein expression and purification

BL21 *E. coli* cells bearing the pGEX constructs were grown at 310 K in 2xYTG medium containing ampicillin 100 μg/ml to an absorbance of 0.6–0.8 (600 nm). Protein expression was induced by adding IPTG (1 mM final concentration) and incubating for 2 h at 310 K. The cell suspension was then centrifuged at 7700×*g* for 10 min at 277 K and the pellet was resuspended in PBS containing the following protease inhibitors: PMSF (1 mM), AEBSF (1 mM), E64 (28 μM), PepstatinA (10 μM), Leupeptin (10 μM) and Benzamidine (1 mM). Lysozyme (100 μg/ml) was then added to the cell suspension, which was incubated in ice for 40 min and frozen at 253 K. After thawing, cells were lysed by sonication. To avoid precipitation, TritonX100 (20% in PBS) was added to a final concentration of 1% and incubated for 30 min with gentle agitation. The cell suspension was centrifuged at 12,000×*g* at 277 K for 30 min. The supernatant was mixed with glutathione-sepharose 4B according to the manufacturer's instructions. GST was finally cleaved by incubating fusion proteins bound on matrix with thrombin for 4 h at room temperature under mild agitation. Slurry was centrifuged at 1000×*g* for 5 min at room temperature and the supernatant was stored at 277 K.

2.4. Spin labeling of RGL2-90 mutants

Wild-type and single-cysteine RGL2-90 mutants (250 μM) were incubated with methanethiosulfonate spin label in 20 mM Mes/150 mM KCl/1 mM EDTA, pH 7.5. The reaction was allowed to proceed at room temperature overnight. Hi-Trap Desalting columns were used to remove unreacted spin label. Protein solutions were concentrated to 250 μM using a SpeedVac SC110 concentrator (Savant). When necessary, sucrose was added to a final concentration of 40% w/v.

2.5. EPR measurements

X-band EPR measurements were performed on an Elexsys E-500 spectrometer (Bruker, Germany). Protein samples of 5 μl (≈250 μM) were loaded in quartz capillaries (0.84 mm o. d. × 0.6 mm i.d.) sealed at one end. All spectra were acquired using a 2-mW incident microwave power, 1G field modulation amplitude and modulation frequency of 100 kHz. Scan width was 100 G and the acquisition parameters were chosen to improve the signal-to-noise ratio without generating line broadening.

2.6. Molecular dynamics simulations

The RGL2-90 sequence was homology-modeled onto the NMR structure of mouse Rlf-RBD (PDB ID 1rlf) using the homology module of the Swiss-Pdb Viewer 3.7 [34] programme. To model a particular spin labeled mutant, the wild-type C649 was replaced by a serine and the amino acid of interest was mutated with a cysteine. The spin label was reacted with this single cysteine in order to obtain the R1 side chain (Scheme 1). In the case of the wild-type system, the spin label was attached to the native cysteine in position 649. Each structure was validated with the PROCHECK software [35] available on the Protein Data Bank website.

Energy minimization, MD and data analysis were performed using GROMACS software [36]. Before performing the molecular dynamics simulations, the position of the inserted R1 side chain was minimized in order to have a reliable local starting structure. All mutants were then solvated in a cubic box of water to form a box large enough to contain the protein and 0.7 nm of solvent on all sides. Periodic boundary conditions were used. Since the wild-type protein is positively charged, when necessary the mutants were neutralized by adding the appropriate number of chloride ions as counterions. After solvation and neutralization, all configurations were energy minimized with the steepest descent method for 1000 steps, to remove bad Van der Waals contacts. A simulation of 10.0 ns was performed with these mutants, using SPC water as solvent [37] and GROMOS87 force field [38], allowing all the polar hydrogen atoms to be included in the calculation. The force field was implemented for the spin label chain with parameters (kindly given by Dr. Ileana Stoica, Cornell University) calculated at the ab initio level using Gaussian 98 software. All simulations were performed with a weak coupling time (0.1 ps) [39] to a bath at a constant temperature of 300 K. Protein, solvent and eventual counterions were coupled to the bath individually. Pressure coupling was also applied to a pressure bath with reference pressure of 1 bar, using a coupling time of 1.0 ps.

A cut-off for non-bonded interactions of 1.0 nm was used in all simulations. The SHAKE algorithm [38] was used to constrain all bond lengths, allowing an integration time step of 2 fs. For the water molecules, the SETTLE algorithm was used [40] to constrain the bond length as well as the bond angle.

Molecular dynamics were analyzed excluding the first 1.5 ns in order to consider only the more stable fragment of simulations. The root mean square deviations (rmsd) for the five mutants calculated over the entire molecular dynamics simulations do not exceed 3.0 Å (data not shown).

3. Results

Since a crystal or NMR structure of RGL2-90 is unavailable, it was necessary to perform a homology modelling structure. Using the BLAST server, the best template to use was the RBD domain of the RalGDS family member Rlf (PDB ID 1rlf) [41] that shares a sequence identity of 95% with RGL2-90. Since a protein structure provides a close general model for other proteins with which its sequence homology is >50% [42], one can infer that the homology modelling structure of RGL2-90 (Fig. 1) is a good starting model for molecular dynamics simulations.

Wild-type RGL2-90 contains only one native cysteine (C649) that was labeled and mobility parameters were determined. Four single cysteine mutants of RGL2-90 (where the native cysteine was substituted by a serine) were then produced starting from Cys-less RGL2-90 and each of them reacted with the spin label to generate proteins containing one nitroxide side chain. Thus, a total of five side chains were analyzed in the present work, two of these at the solvent exposed α-helix surface (C649S/R682R1 and C649S/K686R1 mutants), two in loop motifs (C649S/K666R1 and C649S/L703R1 mutants) and the last one with the reporter group at the N-terminal side of the native protein (C649R1), all represented in Fig. 1. Temperature dependence of the EPR spectra was also investigated to determine whether new modes of motion were excited by an increase in temperature or weather weak interaction could be detected by a decrease in temperature. Fig. 2 shows the root mean square fluctuations (rmsf) relative to

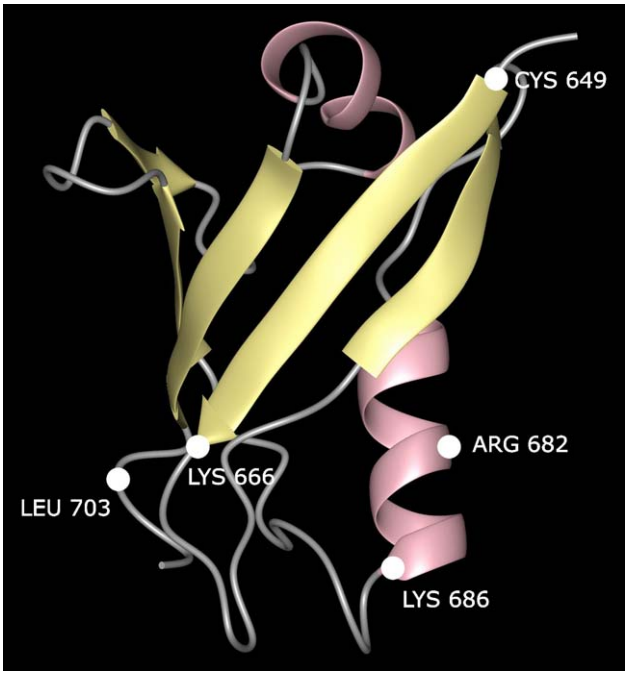

Fig. 1. Ribbon structure of RGL2-90 showing the location of analyzed residues.

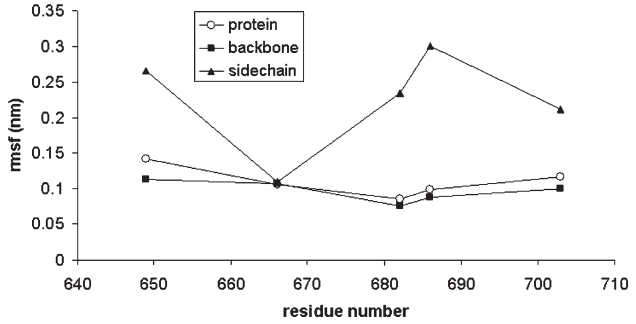

Fig. 2. Root mean square fluctuations for all the mutants.

the starting conformation of protein, backbone and side chain for all the mutants analyzed.

3.1. Comparison between EPR spectra in solution and in 40% sucrose

As the molecular weight of the protein is 10 kDa, the correlation time in solution would be around a few nanoseconds at 298 K. This motion can widely average the hyperfine tensor of the nitroxide at room temperature. The motion of a nitroxide side chain is reflected in the EPR spectral line shape and is related to different correlation times (rotational diffusion of the protein and side chain internal motion). To examine the motion of the nitroxide relative to the protein, it is desirable to reduce the contribution of protein rotation to the spectrum. The EPR spectra were therefore recorded in 40% w/v sucrose solution. The addition of sucrose increases the motion of the protein without affecting the rotation mobility of the side chain at room temperature [10].

The EPR spectra of the mutants C649S/K666R1 and C649S/R682R1 are reported in Fig. 3 as representatives of the two structural categories analyzed, the loop region and α-helix, respectively. The EPR spectra with sucrose at room temperature have been compared (dotted line) with the corresponding EPR spectrum at 273 K without sucrose in both cases (Fig. 3). The C649S/K666R1 spectra are characterized by the classical features of a totally mobile system in both solutions (with and without sucrose). In the case of C649S/R682R1 EPR spectra (Fig. 3), two well resolved components due to different rotamers are evident (see the discussion below). The appearance of the two rotamers for the R1 side chain from the EPR spectra in sucrose at room temperature is evident for the α-helix in respect to the residue in loop. In both cases, the presence of a small amount of free spin label, especially in the spectra of α-helix residue, has to be considered.

3.2. Mobility of nitroxide side chain at solvent-accessible surfaces of α-helices

On the basis of the analysis of the homology modelling structure, two sites (R682R1 and K686R1) were selected so that the nitroxide side chain did not come into contact with other parts of the protein.

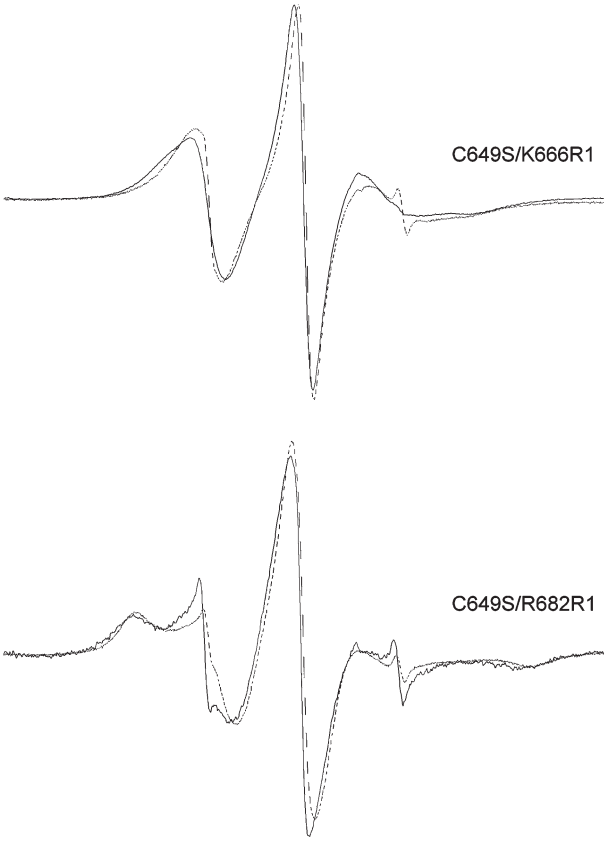

Fig. 3. EPR spectra of C649S/R666R1 and C649S/R682R1 mutants in solution at 273 K compared with the corresponding spectra at room temperature in 40% sucrose solution (dotted line).

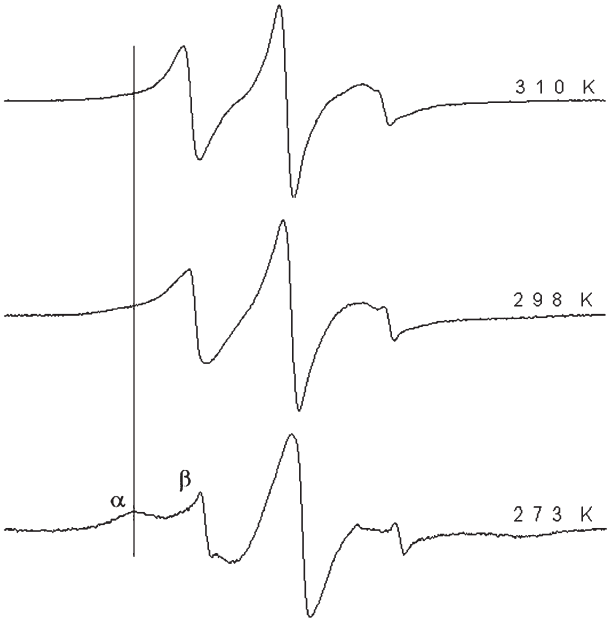

Fig. 4. Variable temperature EPR spectra for the mutant C649S/R682R1 (scan width 100 G). Two spectral components are labeled α (immobile component) and β (mobile component). The presence of a small amount of free spin label is evident.

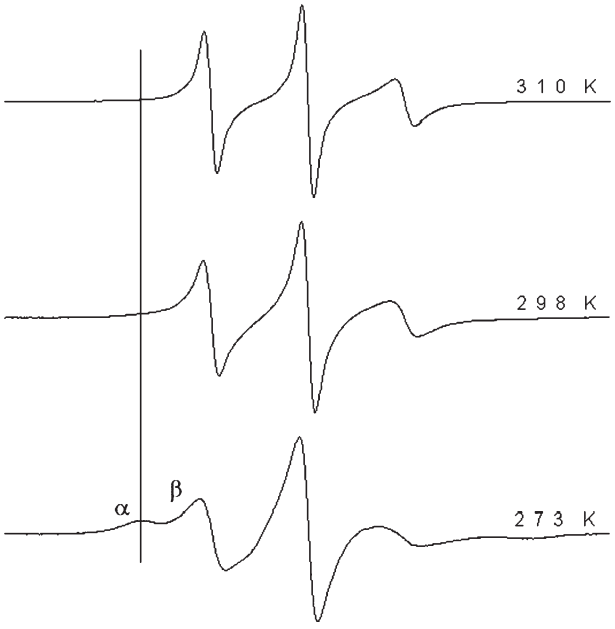

Fig. 5. Variable temperature EPR spectra of mutant C649S/K686R1. Scan width 100 G. Two spectral components are labeled α (immobile component) and β (mobile component). The presence of a small amount of free spin label is evident.

The site R682R1 is located in the middle of helix A and its EPR spectra at variable temperature are reported in Fig. 4. The spectrum at 310 K shows an isotropic motion, but as the temperature decreases the appearance of two well-resolved components, one corresponding to a nitroxide population of lower mobility (labelled α) and the other of higher mobility (labelled β) can be appreciated. A small percentage of these two populations is already visible at low field at room temperature and is completely resolved in the sucrose solution at room temperature (see Fig. 3). The appearance of these two populations is not expected, considering the apparent lack of interaction with the nearest neighbour side chain and the existence of multiple bonds in R1, about which free rotation could occur. Rotation about the disulfide is restricted by a high potential barrier (7 kcal/mol) [43,44] and rotation about the Cα–Cβ bond is hindered by the interaction of the β-carbon with the backbone of the preceding turn. However, the rotations about the Cβ–S_γ, S_γ–S_δ and S_δ–C_ε bonds are expected to give rise to a high mobility (Scheme 1). Mchaourab et al. [10] demonstrated that, at internal helical sites, the rotation about the C_β–S_γ bond is restricted by the presence of disulfide. Thus, the motion that averages the nitroxide magnetic interactions in R1 is the apparent rotation about the terminal bond (χ_5) in the side chain while effective rotations about the C_β–S_γ bond must be largely restricted.

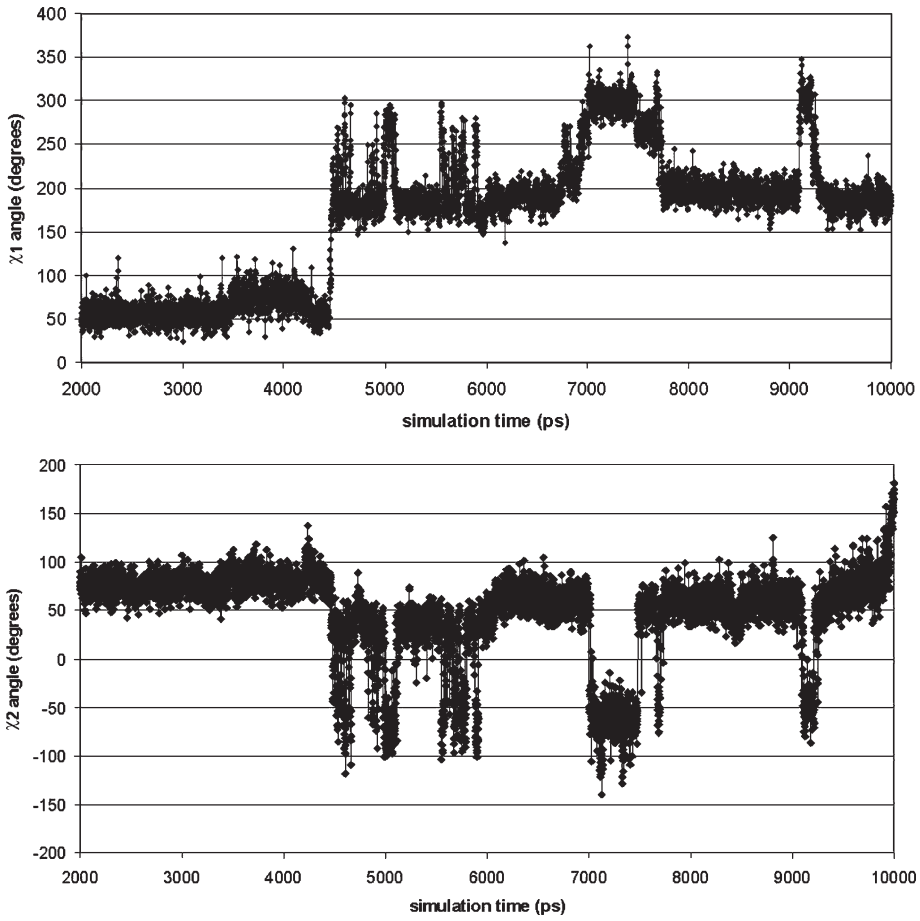

Fig. 6. Time evolution of the dihedral angles χ_1 and χ_2 for C649S/R682R1.

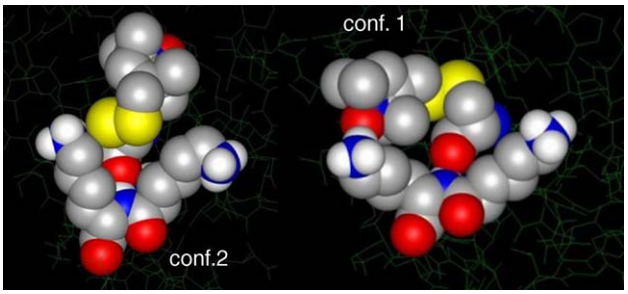

Fig. 7. C649S/R682C conformation 1 (χ_1=188 and χ_2=52) and 2 (χ_1=57 and χ_2=76). The atoms are color coded: red for oxygen, blue for nitrogen, grey for carbon, white for hydrogen and yellow for sulphur. (For interpretation of the references to colour in this figure legend, the reader is referred to the web version of this article.)

The K686R1 site is a fully solvent-exposed C-terminal residue of helix A and it is not expected to have tertiary contacts or other interactions. Variable temperature EPR spectra (Fig. 5) show high mobility and isotropic motion with the appearance of two populations only at 273 K. As the absence of a neighbour side chain at $i\pm4$ is not expected to alter the mobility at this site, the relative mobile spectra observed are due to thermal fluctuations in the backbone around these regions.

When the R1 side chain spectra of these two mutants are compared, it is clear that in position 682 the α population (immobile component) is greater than in position 686. In fact, in this last position, the two components appear only by freezing the sample.

Molecular dynamics simulations support EPR data. In fact, data obtained from C649S/R682R1 MD simulation (see Fig. 6) show two distinct orientations of the disulfide group, corresponding to two conformations of the side chain.

Conformation 1 (χ_1=188 and χ_2=52) corresponds to a situation in the N–O moiety that is hydrogen bound to the amide group of native lysine 686, while conformation 2 (χ_1=57 and χ_2=76) is stabilized by the interaction with the carbon side chain of lysines 685 and 686 (Fig. 7).

Temperature dependence of C649S/R682R1 clearly reveals the two natures of the spectrum (Fig. 4), where one component is essentially immobilized and clearly distinct from the other more mobile one. At higher temperatures, the more immobilized species disappears leaving an apparently single population of spins (see also Fig. 3 where the two populations are visible at room temperature in sucrose). For C649S/K686R1 mutant, molecular dynamics simulations support EPR data; in fact, the root mean square fluctuations (rmsf) for this side chain are higher than for R682R1 site (see Fig. 2). Observation of the evolution of χ_1 and χ_2 angles calculated over the MD simulation

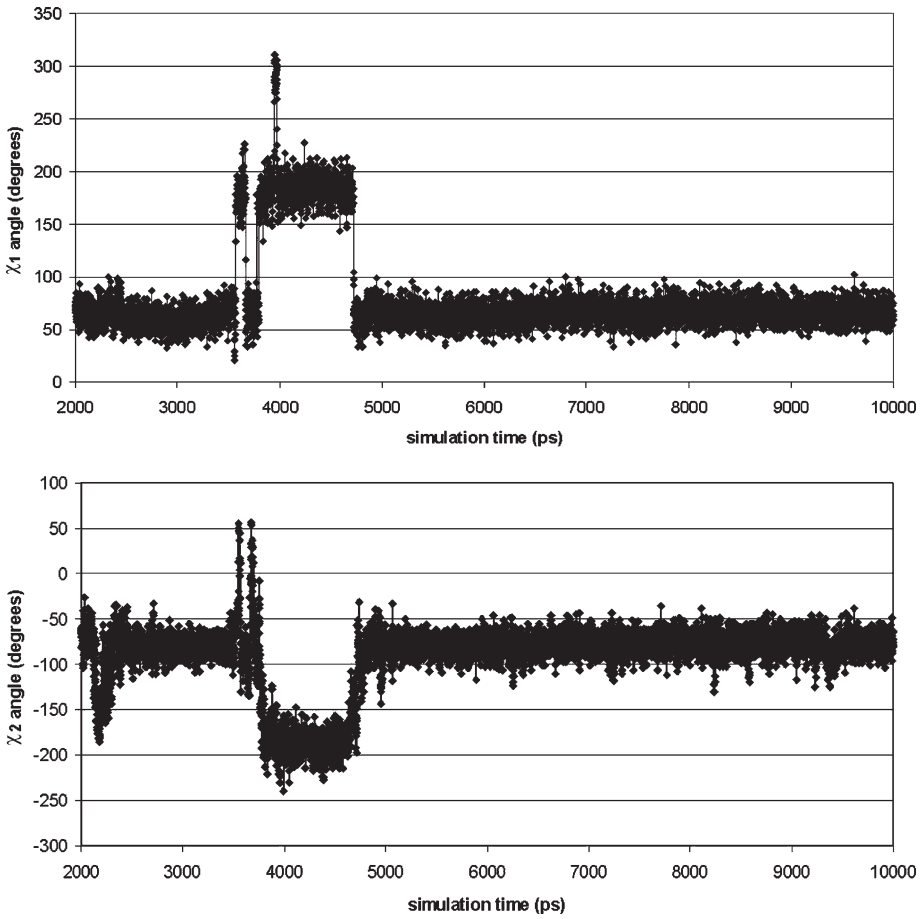

Fig. 8. Time evolution of the dihedral angles χ_1 and χ_2 for C649S/K686R1.

(see Fig. 8) shows that the angles for C649S/K686R1 have a range of mobility similar to C649S/R682R1. Diversities consist in a different orientation due to the different position in sequence compared to C649S/R682R1, and in a more stable geometry of both the principal conformer ($\chi_1 = 66$, $\chi_2 = 287$) and the minor one ($\chi_1 = 184$, $\chi_2 = 175$), although the EPR spectra of C649S/K686R1 reflect a more mobile situation. Differences in the EPR spectra can therefore be attributed to the backbone fluctuations that have more freedom in position 686 than in position 682.

Regarding the R1 side chains in the α-helix, we can therefore conclude that the spectral line shapes reflect motion features of different positions. The residues located in the middle of a helix are characterized by less mobility, and sometimes, as in this case, by stabilization of specific conformers, while the residues at the C-terminal position reveal greater freedom of motion.

3.3. Mobility of nitroxide side chains in loops

Loop regions in proteins connect regular secondary structural elements. In the present study, two different mutants (C649S/K666R1 and C649S/L703R1) and the native domain (C649R1) have been analyzed. The EPR spectra shown in Fig. 9a, b and c panels indicate that the nitroxide is endowed with high mobility in all three cases. Motion is similar to that revealed in the mutant at the C-terminal helix site 686. The increased mobility with respect to the internal helix site 682 can arise from a combination of both the decrease in steric constraints imposed on nanosecond rotation about the C_α–C_β bond in a helix, and large amplitude of fluctuations of the backbone in the nanosecond regime. EPR line shape of the spectrum of C649R1 reflects greater mobility compared with those of K666R1 and L703R1. This is because the native cysteine 649 is the third residue in the sequence and so the backbone has more freedom of motion.

The L703R1 residue is the typical loop residue, with no tertiary interaction and is solvent-exposed. It is inserted in a loop connecting two secondary structures (β-sheet C and β-sheet D). Analysis of the EPR spectra shows that, also in this case, the motion is isotropic and, in particular, its mobility is intermediate between that of C649R1 and K666R1.

Despite the fact that the backbone root mean square fluctuations for L703R1 are similar to those of C649R1, EPR spectra monitor a less mobile situation due to tertiary interactions with the neighbour side chain, although weak.

The MD simulation data on C649S/K666R1, the first residue in the loop between β-sheets A and B, show that the R1 side chain forms hydrogen bonds for 68% of the simulation (data not shown) and makes many contacts with neighbouring residues. In particular, the observed displacement of the side chain atoms suggests that R1 moves coherently with the backbone.

Furthermore, the root mean square fluctuations of the backbone in position 666, together with those in positions 649 and 703, are significant. Therefore, the origin of its isotropic spectrum might be prevalently due to the high fluctuations of the backbone. In conclusion, despite the differences in the steric constraints imposed on the C_α–C_β rotation, C-terminal helix and loop sites have very similar spectra. This suggests that the major contribution to the mobility at these surface exposed sites at room temperature comes from the backbone flexibility.

4. Discussion

To provide an overview of the relationship between structure and mobility, it is convenient to define semiempirical

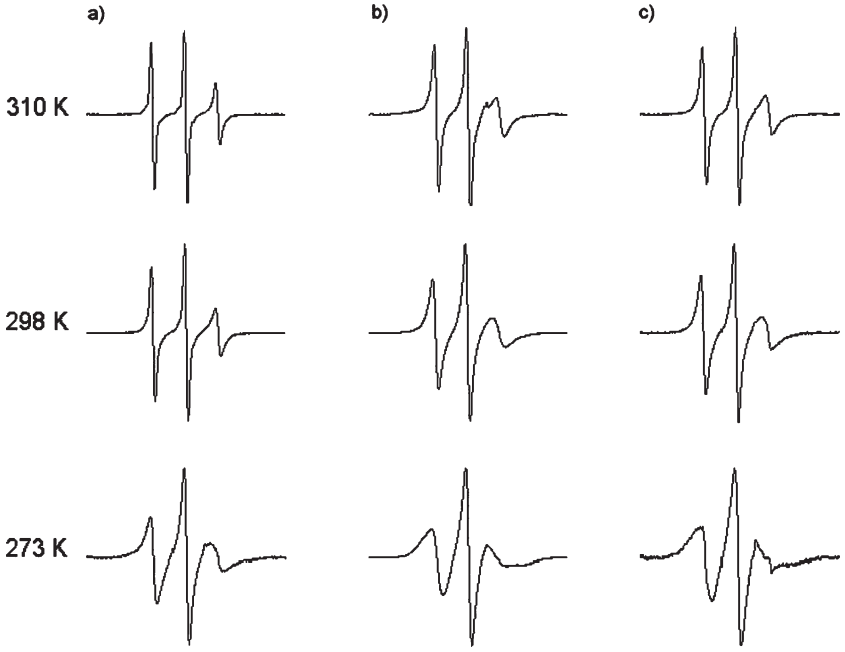

Fig. 9. Variable temperature EPR spectra of the R1 side chains in a loop: (a) C649R1, (b) C649S/K666R1 and (c) C649S/L703R1. Scan width 100 G.

parameters of mobility derived from EPR spectra: namely the spectral breadth, here represented by the spectral second moment ($\langle H^2 \rangle$), and the inverse of peak-to-peak first derivative width of the central resonance (ΔH_{pp}^{-1}) [8]. The numerical values of these quantities at X-band are mainly determined by the degree of averaging of magnetic tensor values. As the frequency of nitroxide rotational motion is reduced, the second moment and the line width increase. Fig. 10 shows a plot of the reciprocal second moment versus the reciprocal central line width for the spectra of R1 side chains representing loop and helix sites. As it is evident in Fig. 10, mobilities are consistent with the tertiary fold of RGL2-90 and there is a linear correlation between the two parameters.

The high isotropic mobility of R1 at solvent exposed loop sites can be explained chiefly on the basis of backbone dynamics, together with the increased freedom of rotation about the C_α–C_β bond in loops compared to internal helical residues. Likewise, the mobility of R1 at solvent exposed C-terminal helix sites can be accounted for by backbone thermal fluctuations. Molecular dynamics simulations of the solution structure suggest that these regions possess considerable backbone motion (see Fig. 2).

The origin of the relatively restricted mobility of R1 at solvent exposed helix surfaces is of some interest because interactions with neighbour side chains are weak. As previously stated [10], replacement of the disulfide in the R1 side chain by a thioether linkage results in a state of high mobility. This indicates that the restricted mobility has its origin in the disulfide bond, which interacts sterically with the hydrogen bound to C_α, and not simply in backbone dynamics, such as those observed in MD simulations. The spectral line shape at 682 site suggests two spin populations. Resolution of these two populations implies an activation barrier for interconversion between populations of at least 7 kcal/mol [10] that constitutes the potential barrier to rotation of disulfide. In this context, the two populations are well resolved thanks to the presence of the disulfide atoms and interactions, shown by molecular dynamics simulations, with amide groups of Lys 685 and Lys 686. These two contributions seem to stabilize the two R1 conformers.

The overall conclusion of the present work is that the position-dependent variation in the EPR line shape of R1 side chain provides a fingerprint of the protein tertiary fold that is consistent with expectations based on data obtained with molecular dynamics simulations. The fact that the results correspond to the structure of the native protein also suggests that the level of structural perturbation, introduced by the R1 side chain, on the protein fold is minimal. The mobility of the R1 side chain in proteins is apparently dominated by tertiary interactions and internal backbone dynamics. The R1 side chain has a relatively unique class of spectral line shapes that identify tertiary interactions. Thus, SDSL-EPR is a powerful tool to map unknown protein structures. In addition to tertiary contact interactions, EPR spectra are clearly modulated by internal fluctuations of the backbone. Assignment of line shape features to this source may be difficult or ambiguous in the case of tertiary interactions or at buried sites, but can be made with some confidence at surface exposed sites.

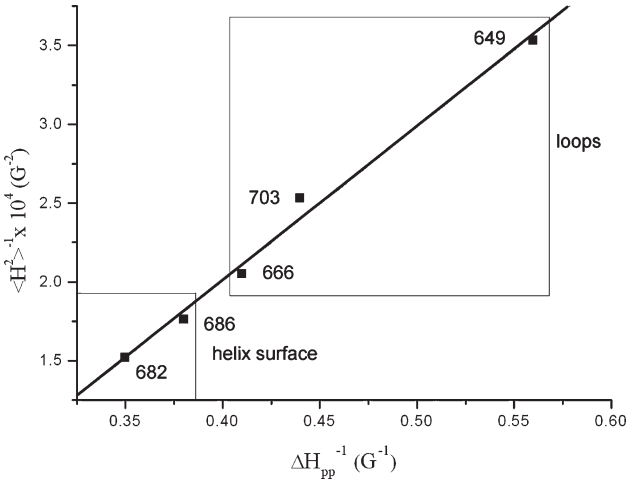

Fig. 10. Reciprocal second moment versus reciprocal central line width calculated from EPR spectra of R1 at the analyzed sites.

The synergistic use of EPR line shape changes combined with molecular dynamics simulations leads to a univocal interpretation of structure and dynamics in solution of biochemically relevant moieties in proteins.

Acknowledgments

This work was supported by the Italian Ministry of University and Research (MIUR)-COFIN, 2002, project no. 2002053415_003. The authors thank Prof. W. Hubbell for useful comments and suggestions, and Dr. I. Stoica for the spin label parametrization values for MD simulations.

References

[1] L.J. Berliner, Spin Labeling Theory and Applications, Academic Press, New York, 1976.
[2] L.J. Berliner, Spin Labeling Theory and Applications II, Academic Press, New York, 1979.
[3] C. Altenbach, S. Flitsch, H.G. Khorana, W.L. Hubbell, Structural studies on transmembrane proteins: 2. Spin labeling of bacteriorhodopsin mutants at unique cysteines, Biochemistry 28 (1989) 7806–7812.
[4] W.L. Hubbell, C. Altenbach, Investigation of structure and dynamics in membrane proteins using site-directed spin labelling, Curr. Opin. Struct. Biol. 4 (1994) 566–573.
[5] W.L. Hubbell, H.S. Mchaourab, C. Altenbach, M.A. Lietzow, Watching proteins move using site-directed spin labeling, Structure 4 (1996) 779–783.
[6] W.L. Hubbell, A. Gross, R. Langen, M.A. Lietzow, Recent advances in site-directed spin labeling of proteins, Curr. Opin. Struct. Biol. 8 (1998) 649–656.
[7] J.B. Feix, C.S. Klug, Spin Labeling: The Next Millennium, Biological Magnetic Resonance, vol. 14, Plenum Press, New York, 1998.
[8] H.S. Mchaourab, T. Kalai, K. Hideg, W.L. Hubbell, Motion of spin-labeled side chains in T4 lysozyme: effect of side chain structure, Biochemistry 38 (1999) 2947–2955.
[9] O.H. Griffith, P.J. Dehlinger, S.P. Van, Shape of the hydrophobic barrier of phospholipid bilayers (evidence for water penetration in biological membranes), J. Membr. Biol. 15 (1974) 159–192.
[10] H.S. Mchaourab, M.A. Lietzow, K. Hideg, W.L. Hubbell, Motion of spin-labeled side chains in T4 lysozyme. Correlation with protein structure and dynamics, Biochemistry 35 (1996) 7692–7704.

[11] H.S. Mchaourab, K.J. Oh, C.J. Fang, W.L. Hubbell, Conformation of T4 lysozyme in solution. Hinge-bending motion and the substrate-induced conformational transition studied by site-directed spin labeling, Biochemistry 36 (1997) 307–316.
[12] G.I. Likhtenstein, Spin Labeling Methods in Molecular Biology, Wiley-Interscience, New York, 1976.
[13] M.D. Rabenstein, Y.K. Shin, Determination of the distance between two spin labels attached to a macromolecule, Proc. Natl. Acad. Sci. U. S. A. 92 (1995) 8239–8243.
[14] J.C. Voss, L. Salwinski, H.R. Kaback, W.L. Hubbell, A method for distance determination in proteins using a designed metal ion binding site and site-directed spin labeling: evaluation with T4 lysozyme, Proc. Natl. Acad. Sci. U. S. A. 92 (1995) 12295–12299.
[15] E.J. Hustedt, A.I. Smirnov, C.F. Laub, C.E. Cobb, A.H. Beth, Molecular distances from dipolar coupled spin-labels: the global analysis of multifrequency continuous wave electron paramagnetic resonance data, Biophys. J. 74 (1997) 1861–1877.
[16] H.J. Steinhoff, N. Radzwill, W. Thevis, V. Lenz, A.A. Brandeburg, G. Dodson, A. Wollmer, Determination of interspin distances between spin labels attached to insulin: comparison of electron paramagnetic resonance data with the X-ray structure, Biophys. J. 73 (1997) 3287–3298.
[17] L.J. Berliner, G.R. Eaton, S.S. Eaton, Distance Measurements in Biological Systems by EPR, Biological Magnetic Resonance, vol. 19, Plenum Press, New York, 2000.
[18] C. Altenbach, T. Marti, H. G Khorana, W.L. Hubbell, Transmembrane protein structure: spin labeling of bacteriorhodopsin mutants, Science 248 (1990) 1088–1092.
[19] D. Greenhalgh, C. Altenbach, W.L. Hubbell, S. Khorana, Locations of Arg-82, Asp-85, and Asp-96 in helix C of bacteriorhodopsin relative to the aqueous boundaries, Proc. Natl. Acad. Sci. U. S. A. 88 (1991) 8626–8630.
[20] C. Altenbach, D. Greenhalgh, H.G. Khorana, W.L. Hubbell, A collision gradient method to determine the immersion depth of nitroxides in lipid bilayers: application to spin-labeled mutants of bacteriorhodopsin, Proc. Natl. Acad. Sci. U. S. A. 91 (1994) 1667–1671.
[21] Z. Farahbakhsh, K.D. Ridge, H.G. Khorana, W.L. Hubbell, Mapping light-dependent structural changes in the cytoplasmic loop connecting helices C and D in rhodopsin: a site-directed spin labeling study, Biochemistry 34 (1995) 8812–8819.
[22] C. Altenbach, K. Yang, D.L. Farrens, Z. Farahbakhsh, H.G. Khorana, W.L. Hubbell, Structural features and light-dependent changes in the cytoplasmic interhelical E-F loop region of rhodopsin: a site-directed spin-labeling study, Biochemistry 35 (1996) 12470–12478.
[23] K. Yang, D.L. Farrens, C. Altenbach, W.L. Hubbell, H.G. Khorana, Structure and function in rhodopsin. Cysteines 65 and 316 are in proximity in a rhodopsin mutant as indicated by disulfide formation and interactions between attached spin labels, Biochemistry 35 (1996) 14040–14046.
[24] D.L. Farrens, C. Altenbach, K. Yang, W.L. Hubbell, H.G. Khorana, Requirement of rigid-body motion of transmembrane helices for light activation of rhodopsin, Science 274 (1996) 768–770.
[25] K. Cai, R. Langen, W.L. Hubbell, H.G. Khorana, Structure and function in rhodopsin: topology of the C-terminal polypeptide chain in relation to the cytoplasmic loops, Proc. Natl. Acad. Sci. U. S. A. 94 (1997) 14267–14272.
[26] J.M. Kim, C. Altenbach, R. Thurmond, H.G. Khorana, W.L. Hubbell, Structure and function in rhodopsin: rhodopsin mutants with a neutral amino acid at E134 have a partially activated conformation in the dark state, Proc. Natl. Acad. Sci. U. S. A. 94 (1997) 14272–14278.
[27] A.P. Todd, J. Cong, F. Levinthal, C. Levinthal, W.L. Hubbell, Site-directed mutagenesis of colicin E1 provides specific attachment sites for spin labels whose spectra are sensitive to local conformation, Proteins 6 (1989) 294–305.
[28] E. Perozo, D.M. Cortes, L.G. Cuello, Three-dimensional architecture and gating mechanism of a K+ channel studied by EPR spectroscopy, Nat. Struct. Biol. 5 (1998) 459–469.
[29] S.N. Peterson, L. Trabalzini, T.R. Brtva, T. Fischer, D.L. Altschuler, P. Martelli, E.G. Lapetina, C.G. Der, G.C. White, Identification of a novel RalGDS-related protein as a candidate effector for Ras and Rap1, J. Biol. Chem. 271 (1996) 29903–29908.
[30] T.H. Fischer, J. Brittain, L. Trabalzini, A.L. Banes, G.C. White, C.J. Smith, T.C. Nichols, The ras-binding domain of ral GDS-like protein-2 as a ras inhibitor in smooth muscle cells, Biochem. Biophys. Res. Commun. 305 (2003) 934–940.
[31] L.E.W. LaConte, V. Voelz, W. Nelson, M. Enz, D.D. Thomas, Molecular dynamics simulation of site-directed spin labeling: experimental validation in muscle fibers, Biophys. J. 83 (2002) 1854–1866.
[32] H.J. Steinhoff, W.L. Hubbell, Molecular dynamics simulation and EPR spectroscopy of nitroxide side chains in bacteriorhodopsin, J. Mol. Liq. 84 (2000) 17–27.
[33] D.J. Schneider, H.J. Freed, in: L.J. Berliner, J. Reuben (Eds.), Spin Labeling: Theory and Applications, Biological Magnetic Resonance, vol. 8, Plenum Press, New York, 1989.
[34] N. Guex, M.C. Peitsch, Swiss-model and Swiss-Pdb Viewer: an environment for comparative protein modelling, Electrophoresis 18 (1997) 2714–2723.
[35] R.A. Laskowski, M.W. MacArthur, D.S. Moss, J.M. Thornton, PROCHECK: a program to check the stereochemical quality of protein structures, J. Appl. Crystallogr. 26 (1993) 283–291.
[36] D. Van der Spoel, A.D. Van Buuren, E. Apol, P.J. Meulenhoff, D.P. Tieleman, A.L.T.M. Sijbers, B. Hess, K.A. Feenstra, E. Lindhal, R. Van Drunen, H.J.C. Berendsen, GROMACS User Manual Version 3.1.1, Groningen, The Netherlands, 2002.
[37] H.J.C. Berendsen, J.P.M. Postma, W.F. van Gusteren, J. Hermans, in: B. Pullman (Ed.), Intermolecular Forces, D. Reidel Publishing Company, Dordrecht, 1981.
[38] W.F. van Gusteren, H.J.C. Berendsen, Gromos-87 Manual, Biomos BV Nijenborgh 4, 9747 AG Grongen, The Netherlands, 1987.
[39] H.J.C. Berendsen, J.P.M. Postma, A. Di Nola, J.R. Haak, Molecular dynamics with coupling to an external bath, J. Chem. Phys. 81 (1984) 3684–3690.
[40] J.P. Ryckaert, G. Ciccotti, H.J.C. Berendsen, Numerical integration of the cartesian equations of motion of a system with constraints: molecular dynamics of *n*-alkanes, J. Comput. Phys. 23 (1977) 327–341.
[41] R.M.F. Wolthuis, B. Bauer, L.J. van't Veer, A.M.M. de Vries-Smith, R.H. Cool, M. Spaargaren, A. Wittinghofer, B.M.T. Burgering, J.L. Bos, RalGDS-like factor (Rlf) is a novel Ras and Rap1A-associating protein, Oncogene 13 (1996) 353–362.
[42] C. Chothia, A.M. Lesk, The relation between the difference of sequence and structure in proteins, EMBO J. 5 (1986) 823–826.
[43] R.R. Fraser, G. Boussard, J.K. Saunders, J.B. Lambert, Barriers to rotation about the sulfur–sulfur bond in acyclic disulfides, J. Am. Chem. Soc. 93 (1971) 3822–3823.
[44] D. Jiao, M. Barfield, J.E. Combariza, V.J. Hruby, Ab initio molecular orbital studies of the rotational barriers and the sulphur-33 and carbon-13 chemical shieldings for dimethyl disulfide, J. Am. Chem. Soc. 114 (1992) 3639–3643.